JACS
JOURNAL OF THE AMERICAN CHEMICAL SOCIETY

Article

pubs.acs.org/JACS

Multidentate Polymer Coatings for Compact and Homogeneous Quantum Dots with Efficient Bioconjugation

Liang Ma,[†,‡,§] Chunlai Tu,[‡,∥,§,○] Phuong Le,[‡,∥] Shweta Chitoor,[‡,∥] Sung Jun Lim,[‡,∥] Mohammad U. Zahid,[‡,∥] Kai Wen Teng,[⊥,◇] Pinghua Ge,[#,◇] Paul R. Selvin,[⊥,#,◇] and Andrew M. Smith*[,†,‡,∥]

[†]Department of Materials Science and Engineering, [‡]Micro and Nanotechnology Laboratory, [∥]Department of Bioengineering, [⊥]Center for Biophysics and Quantitative Biology, [#]Department of Physics, and [◇]Center for the Physics of Living Cells, University of Illinois at Urbana−Champaign, Urbana, Illinois 61801, United States

[○]School of Physical Science and Technology, ShanghaiTech University, 100 Haike Rd., Pudong New Area, Shanghai, 201210, China

Supporting Information

ABSTRACT: Quantum dots are fluorescent nanoparticles used to detect and image proteins and nucleic acids. Compared with organic dyes and fluorescent proteins, these nanocrystals have enhanced brightness, photostability, and wavelength tunability, but their larger size limits their use. Recently, multidentate polymer coatings have yielded stable quantum dots with small hydrodynamic dimensions (≤10 nm) due to high-affinity, compact wrapping around the nanocrystal. However, this coating technology has not been widely adopted because the resulting particles are frequently heterogeneous and clustered, and conjugation to biological molecules is difficult to control. In this article we develop new polymeric ligands and optimize coating and bioconjugation methodologies for core/shell CdSe/$Cd_xZn_{1-x}S$ quantum dots to generate homogeneous and compact products. We demonstrate that "ligand stripping" to rapidly displace nonpolar ligands with hydroxide ions allows homogeneous assembly with multidentate polymers at high temperature. The resulting aqueous nanocrystals are 7−12 nm in hydrodynamic diameter, have quantum yields similar to those in organic solvents, and strongly resist nonspecific interactions due to short oligoethylene glycol surfaces. Compared with a host of other methods, this technique is superior for eliminating small aggregates identified through chromatographic and single-molecule analysis. We also demonstrate high-efficiency bioconjugation through azide−alkyne click chemistry and self-assembly with hexa-histidine-tagged proteins that eliminate the need for product purification. The conjugates retain specificity of the attached biomolecules and are exceptional probes for immunofluorescence and single-molecule dynamic imaging. These results are expected to enable broad utilization of compact, biofunctional quantum dots for studying crowded macromolecular environments such as the neuronal synapse and cellular cytoplasm.

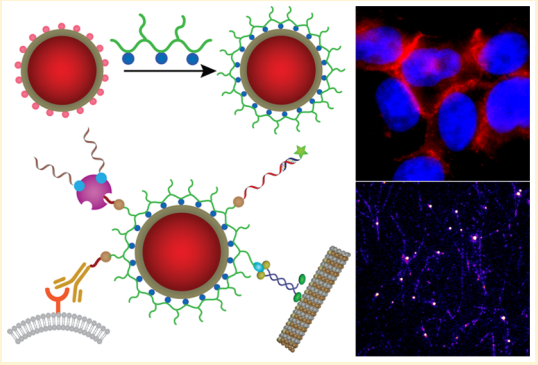

INTRODUCTION

Quantum dots (QDs) are nanocrystals composed of semiconductors with size-tunable optical and electronic properties.[1] These nanoparticles have been diversely employed as light-absorbing components of solar cells,[2] light-emitting components of LEDs and lasers,[3] and fluorescent probes for biomolecular detection and imaging.[4] Their unique properties primarily arise from the quantum confinement effect, in which excited-state charge carriers (electrons and holes) are confined to sizes smaller than their intrinsic dimensions in the bulk semiconductor material.[5] This results in high-efficiency fluorescence emission as well as size-tunable absorption and emission wavelengths. By selecting specific combinations of composition and size, these particles can emit light over an exceptionally broad and continuously tunable spectral range, from the ultraviolet,[6] throughout the visible,[7] and into the near-infrared[8] and mid-infrared.[9] The emission bandwidth is narrow when size distributions are small, and fluorescence quantum efficiencies can approach 100% after epitaxial growth of an insulating shell.[10]

QDs have had a major impact on biomolecular detection and imaging since their first use in cells in 1998.[4,11] When conjugated to bioaffinity molecules such as antibodies, nucleic acids, and ligands, QDs enable multiplexed detection and monitoring of spectrally distinct molecules and processes using a single excitation source.[12] Their fluorescence emission is typically orders of magnitude brighter and more stable than emission from fluorescent dyes and proteins, allowing continuous monitoring of biological processes for long durations at single-particle sensitivity. This latter feature has enabled the understanding of a multitude of new biological

Received: November 26, 2015
Published: February 10, 2016

DOI: 10.1021/jacs.5b12378
J. Am. Chem. Soc. 2016, 138, 3382−3394

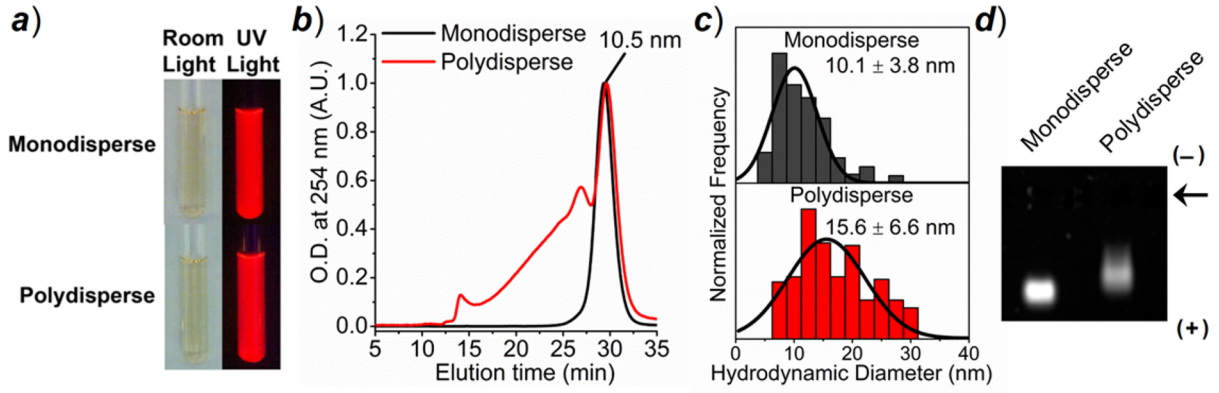

Figure 1. Comparison between multidentate ligand-coated quantum dot samples that are monodisperse or polydisperse. (a) Photographs of a monodisperse sample (top) and polydisperse sample (bottom) under room light (left) or ultraviolet light (right). (b) Gel permeation chromatogram of the two samples. (c) Hydrodynamic size distribution of the two samples measured by single-molecule fluorescence imaging in a mixture of aqueous buffer and glycerol. (d) Gel electrophoresis results for the two samples; the well position is indicated by the arrow, and electrode polarities are indicated as (−) and (+). Detailed synthetic methods are provided in the Experimental Section.

phenomena at the single-molecule level that could not have been readily discerned using conventional techniques and probes.[13]

An ongoing problem in the field of QD-based biomolecular analysis has been the relatively large size of the probes.[14] From commercial suppliers, the hydrodynamic diameter is 15−35 nm, which is much larger than typical globular proteins (∼5−10 nm) that QDs are usually used to analyze. Because of this physical disadvantage, the optical advantages of these probes have not yet been fully exploited for many proposed applications. Large QDs cannot access the crowded neuronal synapse, a 20−30 nm space between connected cells,[15] and are largely immobile in the cellular cytoplasm,[14,16] where macromolecular crowding effects dominate the behavior of colloids. In addition, their large sizes can sometimes impede specific binding to targets,[17] and the multivalent nature of conjugation results in unknown stoichiometry to molecular targets.[18]

Minimizing the QD size has proven to be difficult. The hydrodynamic size derives from a combination of contributions from the "hard" crystalline QD and the "soft" coating that is usually organic. A prototypical core/shell CdSe/$Cd_xZn_{1-x}S$ crystalline QD can be very small (3−4 nm), so the coating has been the primary target for focused engineering strategies for size reduction. As synthesized, QDs are initially coated with aliphatic ligands that render the nanocrystal hydrophobic and insoluble in aqueous solution. Aqueous particles were initially generated using coatings composed of small hydrophilic thiols (e.g., mercaptopropionic acid),[11b,19] silica shells,[11a] and amphiphilic polymers and lipids.[12a,20] Monodentate thiols yield very small colloids, but the nanocrystals are only briefly stable in aqueous solution due to oxidation and weak binding strength.[21] However, recently, our groups engineered these coatings for enhanced stability by adding hydrophobic ligand domains to prevent dissociation from the surface.[15] Silica shells allow diverse chemical functionalization; however, thin shells have been notoriously challenging to generate reproducibly.[22] Amphiphilic polymers and lipids yield robust particles that are the standard for commercial products, but they necessarily add an additional 5−10 nm of hydrodynamic size that is simply too bulky for many applications.[23]

Recently, multidentate and polymeric ligands have been used to prepare compact nanocrystals that are both highly stable and compact.[23,24] These coatings are usually based on linear polymers with three types of pendant functional groups that (1) bind to the nanocrystal surface, (2) extend away from the surface to stabilize the particle in aqueous solution, or (3) enable conjugation to a biomolecule. The resulting colloids are stable for months to years and compatible with harsh purification protocols that destabilize more weakly bound coatings. A variety of polymeric ligands have been reported, synthesized via living radical polymerization, peptide synthesis, or chemical modification of reactive polymers like poly(acrylic acid) or poly(maleic anhydride). Surface-binding groups include thiols,[23,24a−c] imidazoles,[24d−f] and pyridines,[24e] and hydrophilic groups include oligo-ethylene glycol (OEG), polyethylene glycol (PEG)[24a,d,e,g] or zwitterionic betaines,[24b,f] which minimize nonspecific interactions with biological structures such as proteins and cells.

The process of attaching a multidentate polymer to a colloidal surface is not as simple as it is for small molecule ligands.[23] Although the lowest energy conformation of adsorption is through a flat geometry with a maximum number of binding groups associated with the nanocrystal,[25] this conformation can be kinetically difficult to achieve due to competing processes, such as nanocrystal aggregation and polymer cross-linking between particles. The product is often a heterogeneous mixture of small clusters. This outcome is exemplified in Figure 1, demonstrating that QDs coated with multidentate polymers using slightly different procedures (different polymer amount and temperature) can yield monodisperse or polydisperse QDs that are virtually indistinguishable by inspection under room light or ultraviolet light (Figure 1a) and in terms of stability and quantum yield. However, when examined by gel permeation chromatography (GPC, Figure 1b) or by analyzing their diffusion coefficients at the single-molecule level (Figure 1c) it is clear that one of the samples is highly aggregated while the other is monodisperse. In this article, we characterize products generated through a variety of previously described and novel methods and find that nearly all methods yield some degree of nanoparticle aggregation, but importantly this heterogeneity may not be evident from dynamic light scattering (DLS) or gel electrophoresis measurements which provide insufficient resolution of mixed-size samples (Figure 1d and vide infra). For many quantitative imaging and single-molecule analysis applications, achieving a homogeneous, monomeric population is essential,[26]

DOI: 10.1021/jacs.5b12378
J. Am. Chem. Soc. 2016, 138, 3382−3394

Scheme 1. (a) Schematic Illustration of Phase Transfer and Ligand Exchange Processes through Different Tested Methods. (b) Schematic Illustration of Optimized Bioconjugation Methods Using His-Tag-Based Self-Assembly (top) and Copper-Free Click Chemistry (bottom)

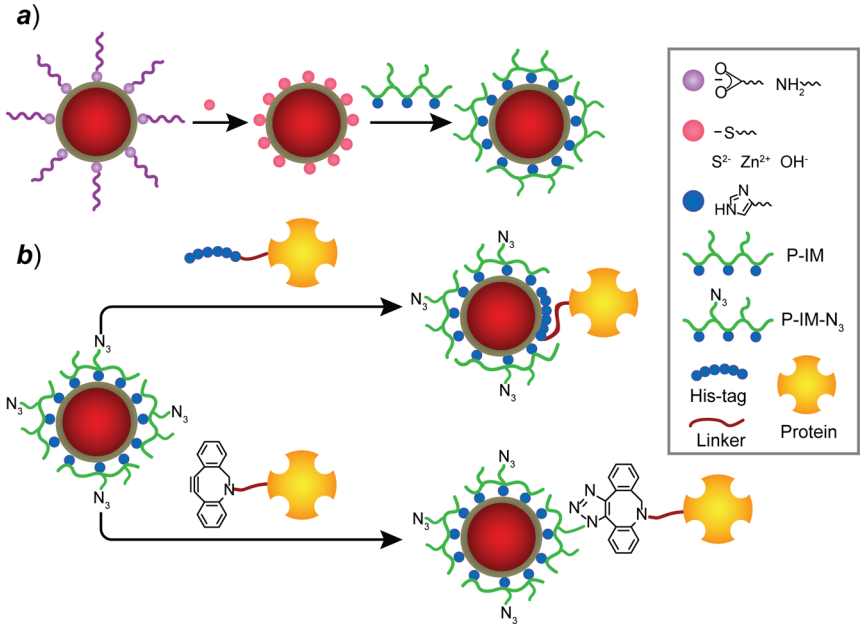

Scheme 2. Synthesis of Multidentate Ligands through Modification of PNAS

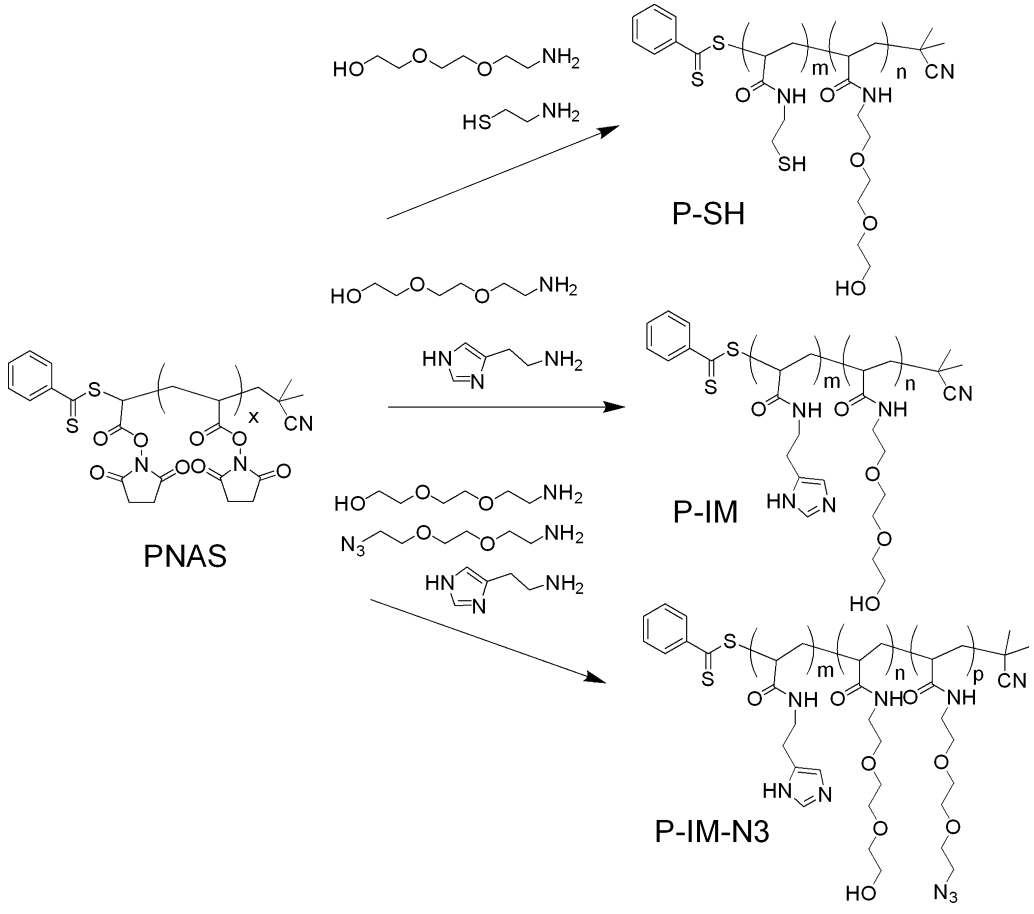

and small populations of clusters skew measurements. To date, ligand exchange processes have not been optimized to maximize monodispersity of QDs coated with multidentate ligands.

DOI: 10.1021/jacs.5b12378
J. Am. Chem. Soc. 2016, 138, 3382–3394

Table 1. Characterization of QD605 Coated with Multidentate Ligands Prepared via Six Different Phase Transfer Methods

method	ligand	polymer	transfer efficiency (%)	quantum yield (%)	size by DLS[a] (nm)	size by GPC[b] (nm)
M1	hydrophobic ligands	P-IM	28.3	21.7	30.8 ± 11.8	>30[c]
		P-SH	31.2	39.0	25.5 ± 7.9	17.5
M2	S^{2-}	P-IM	47.0	18.5	14.9 ± 3.3	>30
		P-SH	32.4	9.0	12.7 ± 2.3	16.3
M3	Zn^{2+}	P-IM	38.6	32.6	53.9 ± 16.4	17.1
		P-SH	41.1	33.2	18.0 ± 7.6	16.5
M4	thioglycerol	P-IM	65.4	35.8	19.2 ± 5.6	15.2
		P-SH	59.1	31.7	17.3 ± 4.6	16.5
M5	mPEG-SH	P-IM	48.5	29.0	14.6 ± 3.3	14.2
		P-SH	55.8	22.3	15.0 ± 3.8	14.6
M6	OH^-	P-IM	66.5	17.8	10.2 ± 2.6	12.5
		P-SH	70.4	16.1	14.0 ± 2.8	N.A.[d]

[a]Hydrodynamic size measured by DLS is the mean diameter from the number distribution. [b]The size measured by GPC is the minimum size among peaks; calculated from calibration curves of proteins with known size. [c]Sizes above 30 nm exceed the GPC column limit. [d]No signal detected.

As depicted in Scheme 1, in this paper we optimized a new methodology for homogeneous and compact polymeric assembly on a QD surface using a two-step process whereby the initial hydrophobic ligands are removed from the nanocrystal surface and replaced with weakly bound ligands or ions. We found that a rapid process using hydroxide ions renders the nanocrystals homogeneously dispersible in polar solvents, in which multidentate polymers can readily displace the weakly bound ions without destabilizing the dispersion. A critical step is to heat the QD−polymer mixture at high temperature (>100 °C) to dissociate small clusters and boost quantum yield, generating homogeneously coated nanocrystals that are exceptionally stable in aqueous solution. We show that this new process substantially improves the quality of the products and is much more rapid than previous multistep coating techniques. Using these new methods, we demonstrate the generation of small, stable, and multicolor QDs in the range of 7.4−11.6 nm with negligible nonspecific association with cells.

We further demonstrate that these nanocrystals can be functionalized with biological molecules using copper-free azide−alkyne click chemistry and self-assembly with molecules containing a His-tag. Unlike frequently used amide-generating bioconjugation reactions (e.g., EDC/NHS chemistry), the reaction yields for these methods are very high, prevent protein cross-linking, and do not require extensive purification.[26a,27] We demonstrate that the QDs can be used for a broad range of biomolecular detection and imaging applications, as DNA conjugates retain their molecular affinity toward hybridization with complementary DNA sequences, antibody conjugates specifically stain cellular antigens, and conjugates to small antibody fragments specifically bind to tagged motor proteins to allow precise measurements of single-molecule motion. We expect that these results will enable the broad adoption of multidentate polymer ligands for quantum dot coating and enhance the utility of QDs for applications requiring highly compact, monodisperse, and stable single-molecule probes.

RESULTS AND DISCUSSION

Design and Synthesis of Multidentate Ligands. Multidentate polymer ligands were designed to allow modular control of chemical structure, a variety of binding groups, and a high graft density of OEG to minimize nonspecific interactions with biological molecules and cells. Polymers were synthesized starting from a linear homopolymer of amine-reactive *N*-hydroxysuccinimide (NHS) functional groups, poly(*N*-acryloyloxysuccinimide) (PNAS). PNAS was synthesized via reversible addition−fragmentation chain transfer (RAFT) polymerization to yield a polymer with 18 900 Da molecular weight, or approximately 110 NHS groups, with a polydispersity index of 1.2 (assessed through GPC).[28] As depicted in Scheme 2, PNAS was reacted with compounds containing primary amines that conjugate to the polymer backbone through an amide bond. The compounds contained either a thiol (cysteamine) or an imidazole (histamine) to bind to QD surfaces or a monoamine triethylene glycol (NH_2-TEG-OH) to render stability in aqueous solution and minimal nonspecific interactions with cells and biological molecules and minimal size. The molar feeding ratio of the binding group compound to the hydrophilic group was 35:65, and separate polymers were created containing thiols (P-SH) or imidazoles (P-IM) in order to compare how the binding group impacts coating. A third polymer (P-IM-N_3) was prepared to contain reactive azide groups using a monoamine, monoazide triethylene glycol (NH_2-TEG-N_3) that replaced 20% of NH_2-TEG-OH in P-IM.

Quantum Dot Nanocrystals. Quantum dots composed of CdSe cores capped with $Cd_xZn_{1-x}S$ shells were synthesized using typical high-temperature organic-phase arrested precipitation and layer-by-layer shell growth methods.[7b] Shells were grown in 0.8 monolayer (ML) increments in order to suppress shell material nucleation and graded in composition from higher CdS content on the CdSe surface to outer layers that were entirely ZnS to aid in stability of the final particle. By tuning both the core size and the shell thickness, the nanocrystals could emit light in the range of 520−610 nm with a fluorescence quantum yield (QY) greater than 40% in hexane or chloroform after purification. For this work, we prepared four batches with different nanocrystal sizes with emission wavelengths indicated by their names: QD525 with 3.3 ± 0.3 nm diameter, QD565 with 4.3 ± 0.5 nm diameter, QD600 with 5.7 ± 0.5 nm diameter, and QD605 with 5.5 ± 0.5 nm diameter; sizes were determined by transmission electron microscopy (TEM) (see Figure S1). After synthesis the nanocrystals were coated with aliphatic ligands such as oleylamine and oleic acid, the predominant ligands in the shell growth solution.

Multidentate Ligand Coating Methods. We found empirically that the attachment of polymeric ligands to QD surfaces is challenging to control and more difficult for

DOI: 10.1021/jacs.5b12378
J. Am. Chem. Soc. 2016, 138, 3382−3394

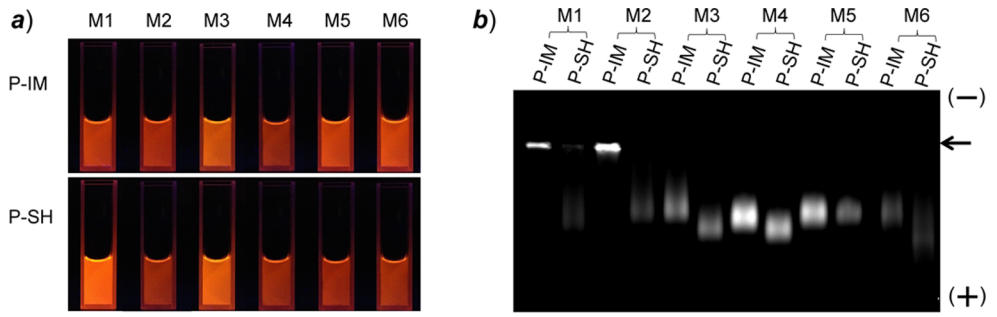

Figure 2. Characterization of QD605 coated with multidentate ligands via six different methods described in Table 1, showing (a) fluorescence images of dispersions in sodium borate buffer (pH = 8.5) and (b) gel electrophoresis images. Black arrow indicates the well position.

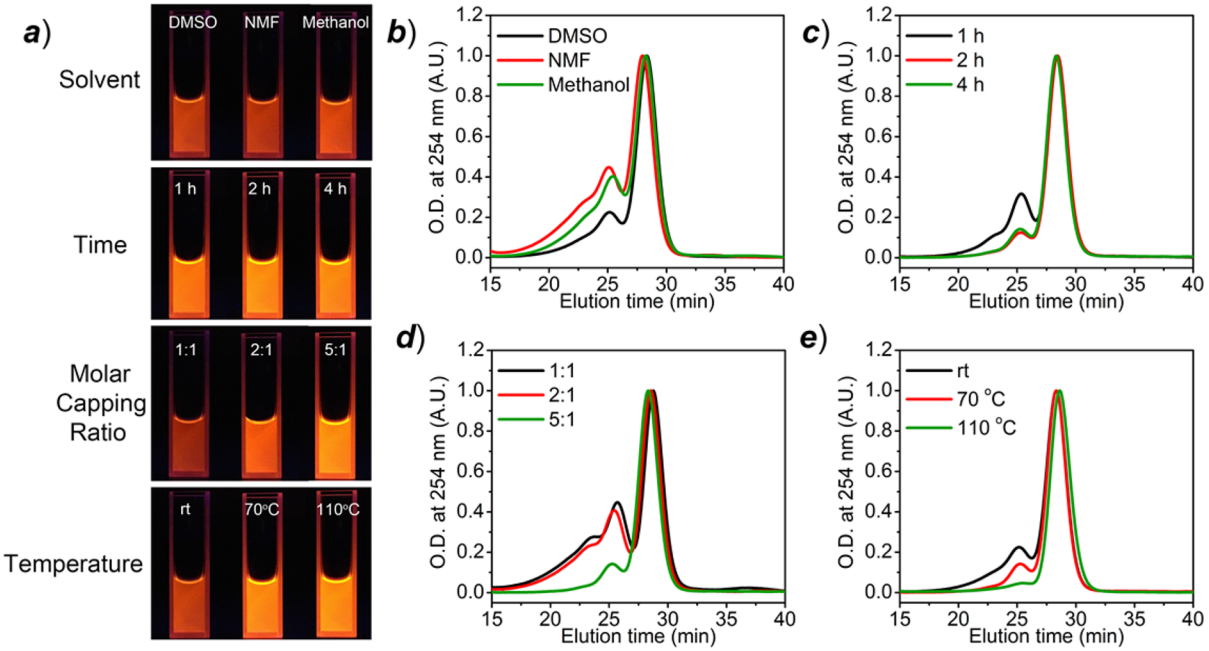

Figure 3. Optimization of coating methods for hydroxide-capped QD605 QDs with P-IM by changing solvents (DMSO, NMF, methanol), reaction time (1, 2, 4 h), molar capping ratio (MCR; 1:1, 2:1, 5:1), and temperature (room temperature, 70 °C, 110 °C). (a) Fluorescent photographs of aqueous P-IM-coated QD605 dispersions under UV excitation. Gel permeation chromatograms of aqueous products using different coating conditions, adjusting (b) solvent, (c) reaction time, (d) MCR, and (e) temperature.

nanoparticles with larger sizes, likely due to the lower surface energy compared with smaller particles that allows competing aggregation processes to dominate. In this work, we focused on maximizing the homogeneity of QD605 coated with P-IM and P-SH by tuning the coating conditions. For homogeneous coating it is critical to judiciously select QD coatings, solvents, and physical conditions that stabilize the surface of the nanocrystal as well as the polymer to prevent aggregation. We found that the most important parameters are the ligands on the surface during exchange and the temperature. First, we tuned the ligands on the nanocrystal surface and mixed the QDs with the multidentate polymeric ligands P-IM or P-SH in solvents optimized to stabilize both the QDs with their initial ligands and the polymer-coated QDs. For each sample, we measured the final transfer efficiency to aqueous solution, fluorescence quantum yield, hydrodynamic size using dynamic light scattering (DLS), gel permeation chromatography (GPC) calibrated with molecular weight protein standards with known diameters, and homogeneity of migration through an agarose-polyacrylamide gel via electrophoresis. The six intermediate ligands and methods (M1−6) are listed in Table 1 and included native hydrophobic ligands in $CHCl_3$ (M1), hydrophilic monodentate ligands that are short chain (thioglycerol, M4) or long chain (PEG-SH, M5), or three ligand-free approaches. The ligand-free coatings were developed by Talapin and co-workers to "strip" the native hydrophobic ligands from the surface, yielding nanocrystals surfaces terminated with sulfide ions (M2), zinc ions (M3), or hydroxide ions (M6).[29]

The results are summarized in Table 1. Importantly, all coatings yield stable colloidal dispersions of QDs in aqueous solution with substantial QY (see Figure 2a). The products were lowest in quality for methods in which the intermediate coatings were hydrophobic ligands, sulfides, and zinc ions (methods M1−M3), which had low transfer efficiencies (<50%), large sizes (>16 nm by GPC), and smeared gel bands (see Figure 2b). The products were particularly aggregated using the P-IM polymer with hydrophobic and sulfide coatings and could not migrate into the gel during electrophoresis. Importantly, for these clustered samples there was little correlation between the average size by DLS and the major population of products observed via GPC. In addition, the degree of band "smearing" showed little correlation with

DOI: 10.1021/jacs.5b12378
J. Am. Chem. Soc. 2016, 138, 3382−3394

GPC analysis, as many of the gel bands appeared to be highly uniform (e.g., M5 P-SH), but all samples tested contained a significant population of clusters revealed by GPC. Smaller sizes and improved transfer efficiencies were obtained with the two thiol ligands and the hydroxide surface coating (methods M4–M6). The results were particularly improved with the hydroxide surface (M6), which yielded the smallest sizes by DLS and GPC and the highest transfer efficiency (>65%). This reagent was also lowest in cost, and the procedure was much more rapid compared with the ones requiring an intermediate thiol. However, this method was only effective with the P-IM polymer, as the thiol-based P-SH polymer yielded products that could not elute through the GPC column, likely due to oxidative disulfide formation in the alkaline coating solution that can cross-link particles. We therefore elected to proceed with further optimization using the imidazole-based polymer and method M6.

Optimization of Polymer Coating via Ligand Stripping. Hydroxide-coated QDs effectively have bare, ligand-free surfaces,[29] with a zeta potential near −26 mV, which provides strong electrostatic repulsion for stabilization in polar solvents such as *N*-methylformamide (NMF) and dimethyl sulfoxide (DMSO). These surfaces provide an ideal substrate for adsorption of polymeric ligands because the particles are highly resistant to aggregation, the inorganic hydroxide adsorbates are readily displaced, and the polar solvent readily dissolves all of the reagents. However, when the coating procedure was performed at room temperature, GPC revealed that despite a small size observed by DLS (10.2 nm), a large fraction of the population was present as small aggregates when using the P-IM polymer. As shown in Figure 3, we further optimized the hydroxide-mediated polymeric coating strategy by adjusting specific reaction parameters (solvent, reaction time, molar capping ratio, and temperature), with outcomes summarized in Table 2. All particles were stable in aqueous solution after purification and yielded fluorescent, transparent dispersions (Figure 3a). The major characteristics for optimization were GPC size and homogeneity, shown in Figure 3b–e. The major peak with the smallest size was deemed to be the unaggregated monomeric QD population, and we quantified its fraction in the population by fitting the chromatograms to a sum of Gaussian peaks, dividing the area of the monomeric QD peak by the total area under the GPC curve. With hydroxide methods, DMSO was the best of three solvents tested for minimizing aggregate peaks (Figure 3b), and a 2 h reaction time was found to be optimal, with no benefit provided by longer times (Figure 3c). Adding excess polymer was found to be beneficial based on the result of varying the molar capping ratio (MCR) which was calculated as the ratio of the number of imidazole groups on the polymer per the total number of QD surface atoms (Figure 3d).[23] To fully minimize the aggregate population, it was most important to use high temperatures for coating (110 °C), which removed small aggregates present, likely due to dissociation of weakly bound conformations of the polymer that were not fully adsorbed (Figure 3e). With high temperatures in DMSO and with excess polymers, the monomeric QDs were present at >96% of the entire population, with a diameter of 10.4 nm by DLS and 11.6 nm by GPC. Sequential optimization of each parameter was critical for minimizing the fraction of aggregate population, and further tweaking of these optimized parameters resulted in nearly 100% monomeric QDs by GPC.

Interestingly, trends in QY in aqueous solution mirrored trends in aggregation: the monomeric percentage correlating with QY with an R^2 of 0.71, indicating that the aggregates likely have lower QY. The QY for QD605 using the optimized method was 47.4%, which is similar to that measured in organic solvents. We conclude that reduced QY in aqueous solution for quantum dots coated with multidentate polymer ligands results in part from small aggregates that are not readily observed with measurement techniques like DLS. Thus, optimization coupled with high-resolution characterization can improve the final optical properties. Using this new methodology, we coated three sizes of QD cores, which yielded high-QY particles that were stable in aqueous solution (Figure 4a) with small sizes (7.4–11.6 nm) by GPC. These hydrodynamic sizes were just 4–6 nm larger than their hard-core TEM sizes. On the basis of the expectation of a ∼5 nm increase in hydrodynamic size by measuring the molecular length of the polymer from the imidazole group to the end of an adjacent OEG, this compact QD is consistent with a flat conformation of polymeric coating on the nanocrystal surface. Their narrow size distributions by

Table 2. Characteristics of P-IM-Coated QD605 with Different Coating Conditions

reaction parameter		QY (%)	size by DLS (*D*, nm)	size by GPC (*D*, nm)	monomeric QDs (%)
solvent[a]	DMSO	20.8	11.6 ± 2.6	11.9	64.0
	NMF	17.8	13.5 ± 3.3	12.1	42.0
	methanol	13.9	11.4 ± 2.5	11.9	45.8
time[b]	1 h	36.4	12.1 ± 2.7	11.9	69.9
	2 h	46.9	12.2 ± 2.4	11.9	92.1
	4 h	34.5	11.0 ± 3.3	11.9	87.9
polymer amount (MCR)[c]	1:1	20.3	11.0 ± 2.9	11.7	39.9
	2:1	25.2	13.1 ± 1.9	11.8	50.0
	5:1	46.9	12.2 ± 2.4	11.9	92.1
temperature[d]	rt	20.8	11.6 ± 2.6	11.9	77.4
	70 °C	34.5	11.0 ± 3.3	11.9	92.1
	110 °C	47.4	10.4 ± 2.4	11.6	95.7

[a]Solvent tuned with fixed reaction time (5 h), MCR (5:1), and temperature (70 °C). [b]Time tuned with fixed solvent (DMSO), MCR (5:1), and temperature (70 °C). [c]MCR tuned with fixed solvent (DMSO), reaction time (2 h), and temperature (70 °C). [d]Temperature tuned with solvent (DMSO), reaction time (2 h), and MCR (5:1).

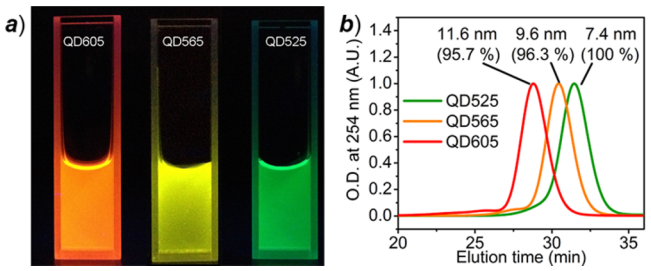

Figure 4. Extension of the optimized coating method for preparation of P-IM-coated QDs with different sizes and colors. Photographs of P-IM-coated QD525, QD565, and QD605 in aqueous solutions under UV excitation (a) and their corresponding gel permeation chromatograms (b).

DOI: 10.1021/jacs.5b12378
J. Am. Chem. Soc. 2016, 138, 3382–3394

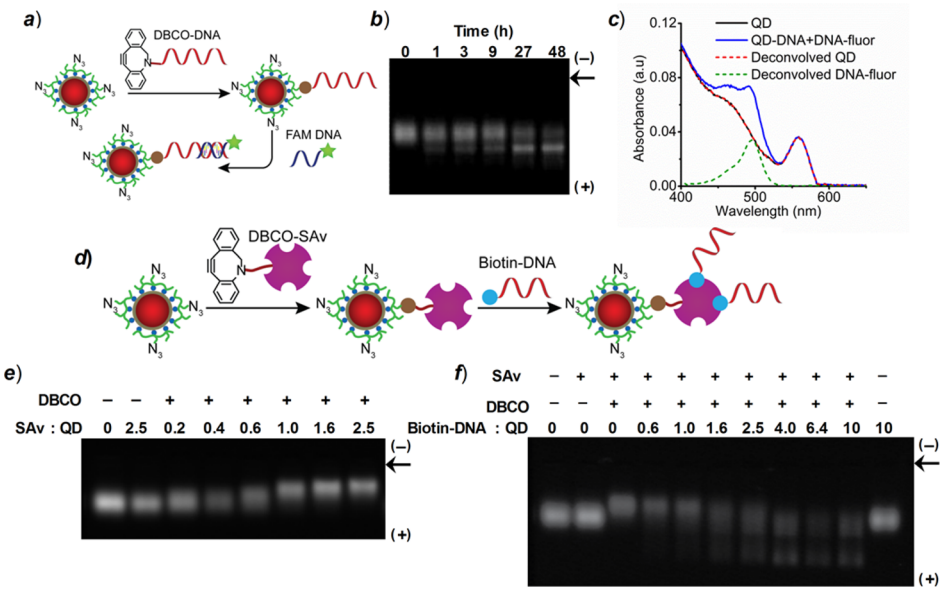

Figure 5. Conjugation of QDs to DNA and proteins through click chemistry is efficient and yields biofunctional conjugates. (a) Schematic illustration of QD−DNA conjugation reactions through copper-free click chemistry using azide-functional QDs and DBCO-terminated single-stranded DNA (90-mer). Conjugation is validated through hybridization with a complementary DNA terminated with fluorescein (21-mer). (b) Gel electrophoresis result for QD−DNA conjugations with a 1:1 molar reaction ratio after different incubation times (0, 1, 3, 9, 27, and 48 h). (c) Absorption spectra of QD, QD−DNA hybridized with DNA−fluor, and the deconvolved spectra of the QD and DNA−fluor. (d) Schematic illustration of QD−streptavidin (SAv) conjugation reactions through copper-free click chemistry and reactions with biotin−DNA. (e) Gel electrophoresis result for SAv−QD reactions using different molar reaction ratios between DBCO−SAv and QD−azide, including a control using SAv without DBCO modification. The reaction was conducted at 4 °C for 24 h. (f) Gel electrophoresis results for QD−SAv−biotin−DNA conjugations using different molar reaction ratios of biotin−DNA to SAv−QDs, including controls using QDs without SAv conjugation. The reaction was conducted at 4 °C for 2 h. Black arrows indicate the well positions.

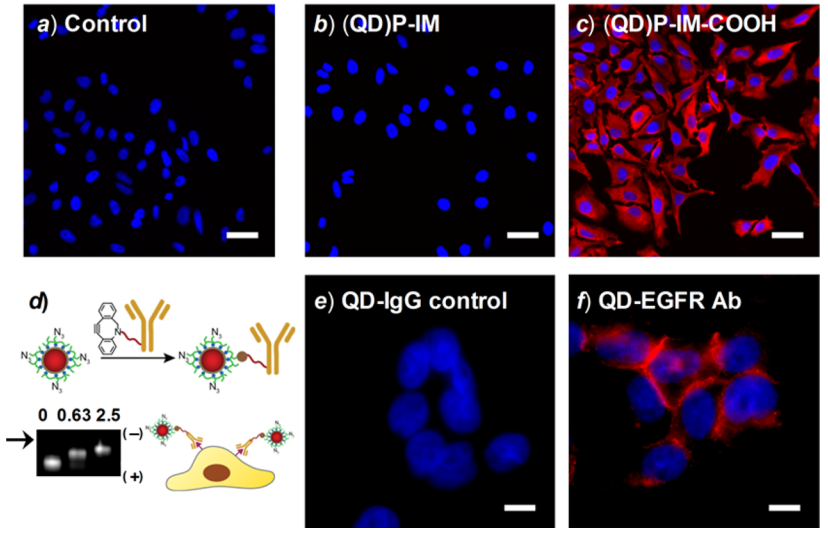

Figure 6. Fluorescence micrographs of fixed and permeablized cells exposed to QDs with different surfaces and bioaffinity molecules validate specific labeling. (a−c) HeLa cells were treated for 1 h at room temperature with (a) no QDs, (b) P-IM-functional QDs, or (c) carboxy-functional QDs. Cells were imaged at 20×; scale bar 50 μm. (d) Schematic illustration of QD−EGFR Ab conjugation and gel electrophoresis validation for different DBCO-Ab:QD reaction ratios (0, 0.63, and 2.5). Black arrow indicates the well position. Specific labeling of EGFR on A431 cells by QD−EGFR Ab conjugates is shown by 100× fluorescence images of fixed and permeabilized A431 cells treated with (e) QDs conjugated to a control IgG or (f) QDs conjugated to an antibody against EGFR. Scale bar 10 μm. Blue color is Hoechst nuclear stain, and red color is QD emission.

GPC (Figure 4b) indicate homogeneity of the monomeric product, comprising 96−100% of the total distribution. The zeta potential for QD605 at pH 7.4 was −11.0 ± 1.2 mV, consistent with previous reports of nanocrystals coated with OEG,[30] and the particles were stable for months without a detectable change in properties, even after harsh purification procedures.

Conjugation to Nucleic Acids and Proteins and Functionality Assays. Compact QDs are similar in hydrodynamic size to many of the biological molecules to which they are conjugated, such as globular proteins. Because simple purification methodologies are usually based on size, it is critical that conjugation reactions go essentially to completion because purification from unreacted biomolecules may not be efficient.

DOI: 10.1021/jacs.5b12378
J. Am. Chem. Soc. 2016, 138, 3382−3394

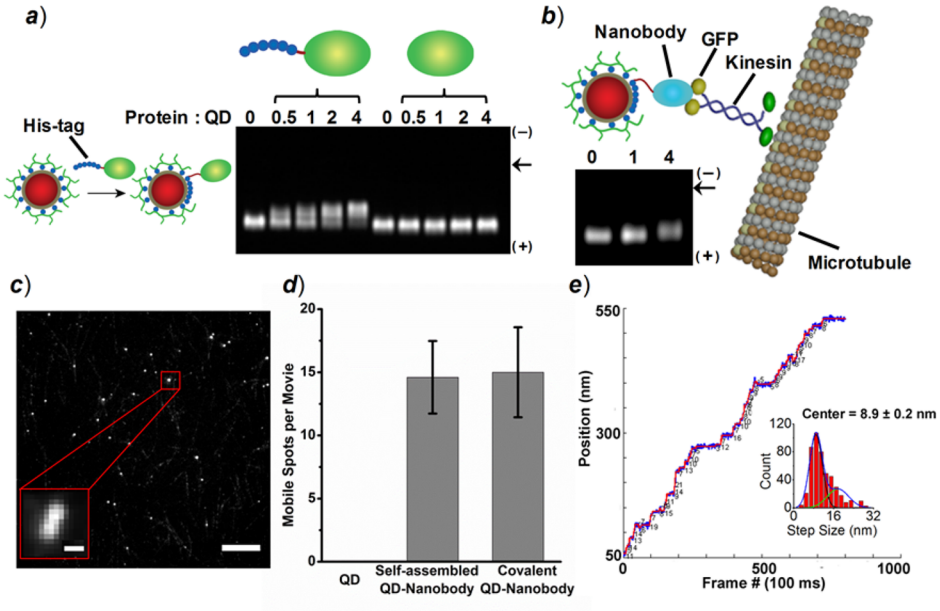

Figure 7. P-IM-coated QDs conjugate to proteins through His-tag linkers, retain protein function, and can be used for single-molecule imaging of motor proteins. (a) (Left) Schematic illustration of self-assembly between P-IM-coated QDs and His-tagged Protein A. (Right) Gel electrophoresis analysis of QDs mixed with His-tagged Protein A or Protein A without a His-tag at different Protein:QD ratios (0, 0.5, 1, 2, 4). (b) Schematic illustration of self-assembly between P-IM-coated QDs and His-tagged nanobodies that can be used to label GFP-kinesin proteins. (Inset) Gel shift for the indicated nanobody:QD ratios (0, 1, 4). Black arrow indicates the well position. (c) Single-molecule fluorescence image from a movie of QD−nanobody-labeled kinesin. Kinesin (K560-GFP) was labeled with the QD−nanobody and imaged while walking in the presence of 800 nM ATP. Dim fluorescent lines are Hilyte488-labeled microtubules (scale bar 8 μm). (Inset) Time-lapsed projection of fluorescent spots over 300 frames (scale bar 0.5 μm). (d) Quantitative analysis of mobile spots per movie using different samples. Error bar indicates standard error (N = 5 for QD−nanobody conjugate; N = 3 for control QD) (e). Example data of a single QD−nanobody-labeled kinesin position analysis with nanometer accuracy. QD position was measured with 100 ms time resolution, and individual traces were fit by a step-finding algorithm. Numbers below the curve are step sizes that the step finding algorithm detected based on the position over time trace. A histogram of step sizes was compiled from 474 steps and 19 traces and fit to a double-Gaussian function (center and 2× center), showing a fundamental step size of 8.9 nm, which is in excellent agreement with the predicted 8.3 nm per step for a kinesin labeled at its center of mass position. The 2× center derives from kinesin taking two steps in succession within the 100 ms time resolution.

We developed two high-efficiency methodologies for our optimized compact particles using His-tag-based self-assembly and azide−alkyne click chemistry. For click chemistry, we prepared a variant of the P-IM polymer for which 20% of the OEG groups were terminated with azides, which can be coupled to strained cyclooctynes such as dibenzylcyclooctyne (DBCO) under ambient conditions without catalysts in aqueous solvents (Figure 5a).[31] QDs coated with this polymer had a similar size and homogeneity as those coated with P-IM (see Figure S2), and upon mixing with biological molecules modified with DBCO, reactions were found to be highly efficient based on mobility shifts in agarose-acrylamide gel electrophoresis. DNA oligomers terminated with DBCO mixed with QDs increased the migration distance of QD (Figure 5b), consistent with an increase in charge. Discrete bands were observed indicative of specific bioconjugate valencies, and after 48 h reaction under ambient conditions, a 1:1 DNA:QD mixture was 64.5% complete, measured by depletion of the unconjugated QD band. The biofunctionality of the attached DNA was verified by mixing these QD−DNA conjugates with a complementary DNA sequence end labeled with a fluorophore (fluorescein; DNA−fluor), which bound to the DNA-conjugated QD but not the QD alone, indicated by their absorption spectra after purification and the deconvolved contributions from the absorbing components (Figure 5c). We also conjugated azide-functional QDs with streptavidin (SAv) modified with DBCO using NHS-DBCO (see Figure 5d). DBCO−SAv specifically conjugated to the QDs based on gel electrophoresis shifts, and a 24 h reaction with SAv:QD molar ratio ≥ 1 was found to be efficient based on the disappearance of the unconjugated QD gel band (Figure 5e). SAv−QD conjugates retained functional binding to biotin, as assessed by mixing with biotin-terminated DNA which yielded a gel shift relative to SAv−QDs (Figure 5f). The two gel bands that appear at higher biotin−DNA:QD ratios (>1.6) may derive from QDs bound to 1 or 2 SAv proteins within the distribution; however, additional analysis is needed to validate this. Nevertheless, it can be deduced that biotin conjugation to SAv−QDs is efficient based on depletion of the SAv−QD band and the absence of additional gel shifts for biotin−DNA reactions with a DNA:QD ratio higher than 4:1 (SAv is a tetramer capable of binding up to 4 biotins but likely cannot be fully saturated in this experiment due to steric and/or electrostatic repulsion[32]). These findings of high reaction efficiencies are important for the wide use of compact QDs, as separation of QD−protein conjugates from unreacted proteins is highly inefficient and low throughput using processes involving chromatography, electrophoresis, and centrifugation.

As shown in Figure 6, we investigated the nonspecific and specific binding of P-IM-coated QDs on fixed cells. The OEG surface was critical for minimizing nonspecific binding, which can be seen by comparing fluorescence images of cells exposed to QDs coated with P-IM or a P-IM-COOH polymer that was nearly identical but for which OEG was replaced with carboxylic acids (compared Figure 6a−c). Using click chemistry, we conjugated (QD)P-IM-N_3 to an antibody (Ab)

DOI: 10.1021/jacs.5b12378
J. Am. Chem. Soc. 2016, 138, 3382−3394

against the epidermal growth factor receptor (EGFR), validated by a gel shift (Figure 6d). The QDs were added to A431 cells expressing human EGFR and bound selectively to the membrane region, unlike QDs conjugated to an isotype control antibody (see Figure 6e and 6f).

Quantum dots coated with P-IM also efficiently self-assembled with proteins expressed as fusions to His-tag, similarly to previous reports using QDs coated with small ligands.[27a] It is surprising that this process occurs efficiently for QDs with a polymeric shell and dense OEG layer.[33] We conjugated QDs to proteins (Protein A) using this mechanism as shown in Figure 7a. Protein binding decreased the gel mobility of QDs with multiple protein conjugate bands observed, and the unconjugated QDs were largely depleted at a Protein:QD ratio of 4:1. Specificity for attachment through the His-tag was verified by control experiments in which Protein A was not labeled with a His-tag, showing no change in gel mobility of the QDs. To verify that they retained their function such that they could be used for single-molecule dynamic imaging applications, we conjugated P-IM-coated QDs to a His-tagged protein called a nanobody, which is a small variant of an antibody (Figure 7b). The nanobody was specific for green fluorescent protein (GFP).[34] The QD−nanobody was mixed with a GFP−kinesin fusion protein, and we applied a well-established single-molecule kinesin motility assay to evaluate whether these QD tags are effective probes for single-molecule analysis of enzymes. As shown in Figure 7c, individual conjugates were readily seen through fluorescence microscopy. Kinesin mobility analysis showed about 15 mobile QDs per movie for QD−nanobody conjugates compared to zero mobile QDs for samples not conjugated to nanobodies (Figure 7d). We compared these results for self-assembled QD−nanobody conjugates with an assay that was identical, except we used QDs−nanobody conjugates prepared through covalent linkage through a PEG spacer,[34] and the results were statistically indistinguishable (Figure 7d). These results demonstrate that P-IM QD probes allow nanobodies bound through His-tags to retain their affinity and do not damage the enzymatic function of kinesin, despite possibly being slightly buried in the OEG shell due to the very short linker between the nanobody and the QD. Due to the very high photostability and brightness of these probes under high-power laser excitation, we were able to analyze the step size of the kinesin motor protein with nanometer accuracy and 100 ms time resolution (Figure 7e). Statistical analysis showed an average step size of 8.9 nm, which is in excellent agreement with the predicted 8.3 nm per step for kinesin labeled at its center of mass position.[35] These very compact and functional conjugates (~12 nm diameter) are thus very suitable for high-sensitivity single-molecule imaging without interference in enzymatic processes.

CONCLUSIONS

In summary, we optimized a facile two-step multidentate ligand-coating strategy for preparing monodisperse and compact QDs. These new QDs are some of the smallest reported to date and exhibit long-term stability and low nonspecific binding on cells due to short-chain OEG tethers to the surface. Most importantly, we validated that the products are homogeneous using gel permeation chromatography and single-molecule imaging and demonstrate how gel electrophoresis and light scattering measurements are insufficient alone to assess the presence of clusters or aggregates in a heterogeneous mixture. We further demonstrated the utility of copper-free click chemistry and His-tag-based self-assembly for efficient bioconjugation to DNA and proteins, without the need for inefficient purification and without altering the function of the conjugated biomolecules. Unlike products from amide-generating reactions, the reactions are highly controllable and proceed effectively to completion. The products were demonstrated to be excellent probes for DNA hybridization, immunofluorescence staining, and single-molecule enzyme imaging, which are some of the most important studies being pursued at present with QDs. We anticipate that the approach presented here will greatly broaden the use of QD with thin polymeric coatings in a wide variety of biological applications, especially single-molecule tracking and quantitative targeting.

EXPERIMENTAL SECTION

Synthesis of Core/Shell CdSe/$Cd_xZn_{1-x}S$ QDs. CdSe cores with a diameter of 2.3 (for QD525 and QD565) or 3.0 nm (for QD600 and QD605) were synthesized using conventional high-temperature-arrested precipitation methods as previously described in the literature.[7b] After purification, $Cd_xZn_{1-x}S$ shells were grown layer-by-layer. In a typical shell growth reaction, a purified core stock in hexane (~1 μmol) was injected into a mixed solvent of ODE (12 mL) and OLA (6 mL) in a 250 mL round-bottom flask and hexane was evaporated under vacuum at 40−50 °C. Then the solution was heated under nitrogen to a temperature used for the first 0.8 ML shell growth (typically 120−130 °C). The first S precursor 0.8 monolayer (ML) was added dropwise within 5−10 min and allowed to react for ~20 min. Equal amounts of Cd/Zn precursor were added in the same manner and allowed to react for another ~20 min to complete the 0.8 ML shell growth. This cycle was repeated while gradually increasing both the Zn ratio (typically from 0.5 to 1) and the reaction temperature (typically from 130 to 200 °C). An aliquot (200 μL) was withdrawn using a glass microsyringe after every 0.8 ML shell growth to monitor the reaction and to measure the extinction coefficient. When the desired emission wavelength was reached, an additional injection of Zn precursor was added, and the particles were annealed for ~20 min in order to render the QD surfaces metal-rich. Specific quantities used for each batch are provided in the Supporting Information. Mixtures were cooled and stored as a crude reaction mixture at −20 °C in the freezer until use.

Synthesis of Polyacrylamido(cysteamine-*co*-TEG) (P-SH). In a 7 mL vial equipped a magnetic stir bar, PNAS (synthesized as described in the literature[28]) (84 mg) was dissolved in dry DMF (1 mL). Monoamine triethylene glycol (NH_2-TEG-OH, 325 μL, 1.0 mM in dry DMF) was added, and the mixture was stirred for 2 h. Cysteamine (350 μL, 0.5 mM in dry DMF) was then added, and the solution was purged with N_2 for 5 min. The reaction was allowed to continue for 24 h at room temperature. DL-Dithiothreitol (8 mg) was then added, and the solution was stirred for 1 h. The solution was diluted 5-fold with an HCl aqueous solution (0.1 mM) and loaded into a dialysis bag (molecular weight cutoff, MWCO = 2 kDa). The polymer was purified by dialysis in HCl solution (1L, 0.1 mM) for 6 h and repeated 3 times. The yellow powder (51 mg) was collected using a lyophilizer (yield 68%). ^{1}H NMR (d_6-DMSO, δ, ppm, 500 MHz): 7.52−7.82 (Ph, br), 4.57 (CH_2, br), 3.14−3.52 (CH_2, br), 2.85 ($CHCH_2$, br), 1.54−2.31 ($CHCH_2$, m), 1.22(CH_3, br).

Synthesis of Polyacrylamido(histamine-*co*-TEG) (P-IM). In a 7 mL vial equipped with a magnetic stir bar, PNAS (84 mg) was dissolved in dry DMF (1.0 mL). NH_2-TEG-OH (325 μL, 1.0 mM in dry DMF) and histamine (175 μL, 1.0 mM in dry DMF) were added, and the solution was purged with N_2 for 5 min. The solution was stirred for 24 h at room temperature. The solution was diluted 5-fold with deionized water and loaded into a dialysis bag (MWCO = 2 kDa). The polymer was purified by dialysis in deionized water for 6 h and repeated 3 times. A yellow solid product (49 mg) was collected after lyophilization (yield 51%). ^{1}H NMR (d_6-DMSO, δ, ppm, 500 MHz):

DOI: 10.1021/jacs.5b12378
J. Am. Chem. Soc. 2016, 138, 3382−3394

7.50−7.93 (Ph, IM, br), 4.58 (CH_2, br), 3.18−3.47 (CH_2, br), 2.81 ($CHCH_2$,br), 1.47−2.07 ($CHCH_2$,m), 1.31 (CH_3,br).

Synthesis of Polyacrylamido(histamine-*co*-TEG-*co*-azido-TEG) (P-IM-N_3). In a 7 mL vial equipped with a magnetic stir bar, PNAS (84 mg) was dissolved in dry DMF (1.0 mL). Then 2-[2-(2-azido-ethoxy)ethoxyl]ethylamine (N_3-TEG-NH_2, 100 μL, 1.0 mM in dry DMF), NH_2-TEG-OH (225 μL, 1 mM in dry DMF), and histamine (175 μL, 1.0 mM in dry DMF) were added, and the solution was purged with N_2 for 5 min. The solution was stirred for 24 h at room temperature and then diluted 5-fold with deionized water and loaded into a dialysis bag (MWCO = 2 kDa). The polymer was purified by dialysis in deionized water for 6 h and repeated 3 times. A yellow solid product (62 mg) was collected after lyophilization (yield 56%).[1] ^{1}H NMR (d_6-DMSO, δ, ppm, 500 MHz): 7.45−7.93 (Ph, br), 3.21−3.47 (CH_2, br), 2.80 ($CHCH_2$,br), 1.51−1.93 ($CHCH_2$,m), 1.20(CH_3,br).

Polymer Coating Methods. CdSe/$Cd_xZn_{1-x}S$ QDs in the crude reaction mixture were purified (more details can be found in SI), and the solution was centrifuged to remove possible aggregates. The general procedures for six different phase transfer methods used in this work are described as follows, and additional details are listed in the Supporting Information.

Method 1 (Hydrophobic Ligand Surface). Hexane was removed from a dispersion of QD605 by evaporation, and the nanocrystals were redispersed in $CHCl_3$. Multidentate ligands P-IM or P-SH (5 equiv of binding group per QD surface atom) dissolved in $CHCl_3$ were added under N_2 atmosphere. The reaction was allowed to proceed for 10 min at room temperature. Methanol was then added, and the reaction was continued for 20 min under N_2 atmosphere. QDs were collected by precipitation with hexane. The nanocrystals were purified by dialysis (MWCO = 50 kDa) to remove residual organic solvent and excess polymers, concentrated by centrifugal filtration (MWCO = 50 kDa), and stored in sodium borate buffer (50 mM, pH 8.5) at room temperature.

Method 2 (S^{2-} Surface). An aqueous solution of $(NH_4)_2S$ (40%) was added to a biphasic mixture of NMF and hexane containing QD605. The mixture was stirred vigorously until complete phase transfer to the NMF phase. Hexane was removed, and the NMF layer containing the QDs was washed with hexane twice, followed by precipitation with ethyl acetate and centrifuging to collect the QDs. The QDs were resuspended in NMF. A solution of P-IM or P-SH in NMF was added dropwise into the solution under stirring and N_2 atmosphere. The reaction was allowed to proceed at room temperature for 24 h. The nanocrystals were purified and stored in the same way as Method 1.

Method 3 (Zn^{2+} Surface). QDs with a S^{2-} surface in NMF from Method 2 were mixed with a solution of $Zn(Ac)_2$ in formamide and stirred for 5 min. The QDs were collected by precipitation from toluene and redispersed in NMF. A solution of P-IM or P-SH in NMF was added dropwise into the QD−NMF solution while stirring. The solution was bubbled with N_2 for 5 min, and the reaction was allowed to proceed at room temperature for 24 h. The nanocrystals were purified and stored in the same way as Method 1.

Method 4 (Thioglycerol Surface). Hexane was removed from a dispersion of QD605 by evaporation. Pyridine was added in a N_2 atmosphere, and the solution was stirred at 80 °C for 2 h. Then thioglycerol was added and stirred at 80 °C for an additional 2 h. Triethylamine was added after the solution was cooled to room temperature and stirred for 30 min. The QDs were precipitated by slow addition into a acetone/hexane mixture and collected by centrifugation. The obtained QDs were homogeneously dispersed in DMSO. A DMSO solution of P-IM or P-SH was added dropwise to the QDs while stirring in an N_2 atmosphere. The reaction was then heated to 80 °C under N_2 for 1.5 h. The nanocrystals were purified and stored in the same way as Method 1.

Method 5 (mPEG-SH Surface). A hexane dispersion of QDs was diluted with $CHCl_3$, and a solution of mPEG-SH in $CHCl_3$ (5000 per QD) was added and stirred for 3 h at room temperature. The solvent was evaporated, and the QDs were dispersed in methanol and bubbled with N_2 for 3 min. A methanol solution of tetramethylammonium hydroxide (TMAH, 25 wt %) was added with mPEG-SH in the same molar quantity. The reaction was allowed to proceed for 2 h at 60 °C under N_2 atmosphere. The QDs were collected by precipitation and redispersed in DMF. P-IM or P-SH was added dropwise into the QDs solution with stirring in a N_2 atmosphere. The reaction was allowed to proceed at room temperature for 24 h. The nanocrystals were purified and stored in the same way as Method 1.

Method 6 (OH^- Surface). A methanol solution of TMAH (25%) was added to a biphasic mixture of NMF and a hexane suspension of QD605. The suspension was stirred vigorously for 1 h until the QDs were completely transferred to the NMF phase. Hexane was removed, and the NMF solution was washed with hexane twice. Residual hexane and methanol were evaporated under vacuum. A solution of P-IM or P-SH in NMF was added dropwise into the solution under stirring and N_2 atmosphere. The reaction was allowed to proceed at room temperature for 24 h. The nanocrystals were purified and stored in the same way as Method 1.

Optimization of Method 6. *Solvent.* The QD605 NMF solution obtained in Method 6 (0.2 mL, 10 μM) was diluted with DMSO (0.4 mL), NMF (0.4 mL), or methanol (0.4 mL). Then P-IM (3.8 mg, 5 equiv of surface atoms of QDs) dissolved in the corresponding solvent (0.2 mL) was added while stirring in a N_2 atmosphere. The reaction was stirred at 70 °C for 5 h. The nanocrystals were purified and stored in the same way as Method 1.

Time. The QD605 NMF solution obtained in Method 6 (0.2 mL, 10 μM) was diluted with DMSO (0.4 mL). Then a DMSO solution of P-IM (5 equiv of surface atoms of QDs, 19 mg/mL, 0.2 mL) was added while stirring in a N_2 atmosphere. The reaction was stirred at 70 °C for 1, 2, or 4 h. The nanocrystals were purified and stored in the same way as Method 1.

Molar Capping Ratio. The QD605 NMF solution obtained in Method 6 (0.2 mL, 10 μM) was diluted with DMSO (0.4 mL). Then a DMSO solution of P-IM (1, 2, and 5 equiv of surface atoms of QDs) was added while stirring in a N_2 atmosphere. The reactions were carried out at 70 °C for 2 h. The nanocrystals were purified and stored in the same way as Method 1.

Temperature. The QD605 NMF solution obtained in Method 6 (0.2 mL, 10 μM) was diluted with DMSO (0.4 mL). Then a DMSO solution of P-IM (5 equiv of surface atoms of QDs, 19 mg/mL, 0.2 mL) was added while stirring in a N_2 atmosphere. The solution was stirred at room temperature, 70 °C, or 110 °C for 2 h. The nanocrystals were purified and stored in the same way as Method 1.

Synthesis of (QD525)P-IM, (QD565)P-IM, and (QD605)P-IM. The synthesis procedures for (QD525)P-IM, (QD565)P-IM, and (QD605)P-IM were identical except that the number of surface atoms was different between the different QDs due to different diameters. NMF solutions (0.2 mL) of hydroxide-coated QDs obtained through Method 6 (QD605, 2.0 nmol; QD565, 5.1 nmol; QD525, 8.7 nmol) were diluted with DMSO (0.4 mL). Then P-IM DMSO solution (5 equiv of surface atoms of QDs, 19 mg/mL, 0.2 mL) was added while stirring in a N_2 atmosphere. The solution was stirred at 110 °C for 2 h. The QDs were further purified by dialysis to remove organic solvents and unreacted polymer and concentrated by centrifugal filtration. For QD605 and QD565, the MWCO of the dialysis bag and centrifugal filter was 50 kDa. For QD525, the MWCO was 30 kDa. The obtained QDs were stored in sodium borate buffer (50 mM) for use and characterization. The procedures were identical when using the P-IM-N_3 polymer.

Synthesis of Monodisperse and Polydisperse QDs. QD cores with 720 nm emission were chosen for this sample so that we could achieve the highest signal-to-noise ratio in single-molecule imaging experiments for hydrodynamic size analysis with maximum accuracy and synthesized according to our previous publication.[7b] The monodisperse and polydisperse samples were prepared using identical cores and identical procedures except using different molar capping ratios and coating temperatures during polymer attachment. For both, NMF dispersions (0.255 mL) of hydroxide-capped QDs (1 nmol) obtained through Method 6 were diluted with DMSO (0.75 mL). For monodisperse samples, a DMSO solution of P-IM (12 mg/mL, 33 μL) was added at a molar capping ratio of 1.5 while stirring under a

DOI: 10.1021/jacs.5b12378
J. Am. Chem. Soc. 2016, 138, 3382−3394

nitrogen atmosphere. The solution was stirred at 110 °C for 2 h. For polydisperse samples, the molar capping ratio was 0.5 and the temperature was 70 °C. All other conditions were identical, and the QDs were purified and concentrated using the same procedure described in Method 1 above.

Conjugation of DBCO−DNA to P-IM-N_3-Coated QDs. Dibenzocyclooctyl (DBCO) terminated oligonucleotide probe (length 90 bp) was purchased from a commercial vendor (Integrated DNA Technologies, Coralville, IA) with HPLC purification. The sequence used was/5′-DBCO-triethylene glycol (TEG)/$(T)_{68}$ TAG CCA GTG TAT CGC AAT GAC G-3′. Azide-functionalized QD565 in 50 mM sodium borate buffer was reacted with DBCO−DNA at a molar ratio of 1:1 QD:DNA. Sodium chloride at a final concentration of 25 mM was added to the reaction mixture to reduce electrostatic repulsion and achieve higher conjugation to QDs. The reaction was performed at room temperature on a vibratory shaker (750 rpm). Conjugation was measured using electrophoresis in hybrid polyacrylamide-agarose gels (2% polyacrylamide and 0.5% agarose).

Hybridization of DNA−Fluor to QD−DNA. Fluorescein-modified oligonucleotides (Integrated DNA technology, Coralville, Iowa) were used to confirm that DBCO DNA-conjugated QDs retained their capacity for hybridization. The sequence used was 5′-6-fluorescein amidite (FAM)/CGTCATTGCGATACACTGGCT-3′. Briefly, An excess of DNA−fluor (15 per QD) was added to QD−DNA (prepared with a 4:1 DBCO−DNA excess, reacted for 72 h in 25 mM sodium chloride). Sodium chloride at a final concentration of 0.1 M was then added. The reaction was performed at room temperature for 3 h on a vibratory shaker (750 rpm). Unhybridized DNA−fluor was removed using a 50-kDa MWCO centrifugal filter. Conjugation was confirmed using UV−vis absorption.

Conjugation of Streptavidin to P-IM-N_3-Coated QDs. Streptavidin (Life Technologies, Grand Island, NY) was conjugated to azide-functionalized QD565 using DBCO-sulfo-NHS ester. Briefly, Streptavidin was reacted with a 5-fold molar excess of DBCO-sulfo-NHS ester on ice for 2 h. This DBCO−SAv was purified using a centrifugal filter (MWCO = 30 kDa) at 4 °C. To conjugate azide-functionalized QD565 with DBCO−SAv, azide-functionalized QD565 in 50 mM sodium borate was transferred to PBS using a centrifugal filter (MWCO = 50 kDa) and mixed with different ratios of DBCO−SAv at 4 °C for 24 h. The reaction was quenched by adding a 50-fold molar excess of 2-azidoacetic acid on ice for 15 min. The conjugation was confirmed using electrophoresis in hybrid polyacrylamide-agarose gels (2% polyacrylamide and 0.5% agarose) at 4 °C.

Conjugation of Biotin−DNA to SAv−QDs. Biotin-labeled DNA (Integrated DNA Technologies) was used to confirm streptavidin conjugation to QDs. The sequence used was 5′-Biotin/$(T)_{68}$ TAG CCA GTG TAT CGC AAT GAC G-3′. Briefly, SAv−QD (1:1 molar ratio of DBCO−SAv:QD) was incubated with different ratios of biotin−DNA at 4 °C for 2 h. Conjugation was measured using electrophoresis in hybrid polyacrylamide-agarose gels (2% polyacrylamide and 0.5% agarose) at 4 °C.

Conjugation of Antibodies to P-IM-N_3-Coated QDs. Mouse antihuman EGFR antibody (BD Biosciences, San Diego, CA) and mouse IgG Isotype Control (ThermoFisher Scientific, Waltham, CA) were conjugated to P-IM-N_3-coated QDs. Briefly, sodium azide was removed from the stock antibody using a 50 kDa MWCO centrifugal filter and then reacted with a 50-fold molar excess of DBCO-sulfo-NHS ester on ice for 2 h. Unreacted reagents were quenched by adding Tris-HCl (50 mM) on ice for 15 min and removed using a centrifugal filter. P-IM-N_3-coated QD565 in 50 mM sodium borate was transferred to PBS using a centrifugal filter and then incubated with different ratios of DBCO-activated antibody at 4 °C for 7 h. The reaction was quenched by adding a 50-fold molar excess of 2-azidoacetic acid on ice for 15 min. Conjugation was confirmed using electrophoresis in hybrid polyacrylamide-agarose gels (2% polyacrylamide and 0.5% agarose).

Evaluation of Nonspecific Binding to Cells. HeLa cells (ATCC #CCL2) were cultured in Eagles' Minimum Essential Medium (EMEM) with 10% fetal bovine serum (FBS) and 1% penicillin/streptomycin (P/S) at 37 °C with 5% CO_2. Cells were seeded at a 5 × 10^4 cell/well density on 12 mm circular coverglass in 24 well plates and cultured for 24 h. The cells were washed three times with PBS before fixation with freshly prepared 4% paraformaldehyde (PFA) for 20 min at room temperature. The cells were washed with PBS three times and permeabilized with 0.1% Triton X-100 in PBS for 20 min. The cells were washed with PBS three times and blocked with 1 wt % bovine serum albumin (BSA) for 1 h. The cells were washed with PBS three times, and 40 nM dispersions of (QD)P-IM or (QD)P-IM-COOH in 1 wt % BSA solution were added to the wells and incubated for 1 h at room temperature. Control experiments were carried out by incubating cells without QDs. The cells were washed three times with PBS to remove unbound QDs, and the nuclei were stained with Hoechst 33258 dye (2 μg/mL). The coverglass with cells was then mounted with 90% glycerol in PBS on a glass slide and sealed with nail polish. The cells were imaged immediately on a Zeiss Axio Observer Z1 inverted microscope (Zeiss, Oberkochen, Germany) with an EC Plan-Neofluar 20 × 0.50 NA air microscope objective. Hoechst signal was imaged using 100 W halogen lamp excitation with a 365 nm excitation filter and 445/50 nm emission filter; QDs were imaged using a 488 nm laser excitation and 600/37 nm bandpass emission filter. Images from the control and QD samples were collected using the same imaging conditions.

Immunofluorescence Staining Using QD−Ab Conjugates. A431 cells (ATCC #CRL-1555) were cultured in Dulbecco's Modified Eagle Medium (DMEM) supplemented with 10% FBS and 1% P/S, seeded at a density of 5 × 10^4 cells/well in a labtek glass-bottom 8 well chamber, and incubated at 37 °C with 5% CO_2 for 20 h. The cells were then fixed with 4% PFA for 20 min, permeabilized with 0.1% (v/v) Triton X-100 for 20 min, and blocked with 1% BSA for 1 h. The cells were then incubated with 10 nM QD565-EGFR antibody conjugate in 1% BSA at a temperature for 30 min and stained with 2 μg/mL of Hoechst for 10 min. All treatments were carried out at room temperature. The samples were imaged immediately using a 100× 1.45 NA alpha Plab-Fluar oil immersion objective on a Zeiss Axio Observer Z1 inverted microscope. Hoechst signal was collected as described above; QD565 signal was imaged using a 488 nm laser excitation and a 562/40 nm bandpass emission filter. Images from the QD565-IgG control conjugate and QD565-EGFR antibody conjugate samples were collected using the same imaging conditions.

Expression and Purification of Nanobody. The expression and purification protocol and vector information on His-tagged GFP-binding nanobody has been previously published.[34] In short, the nanobody was expressed in BL21 cells for 4 h at room temperature. The cells were then pelleted and lysed using 1 mg/mL lysozyme and sonication. The lysate was pelleted by centrifugation at 15 000*g* for 30 min. The supernatant was collected and added to a nickel affinity resin. The nanobody, nickel resin mixture was incubated at 4 °C for 1.5 h while shaking. Flow through was discarded, and the nanobody was eluted using a gradient of imidazole buffer from 50 to 250 mM.

Conjugation of His-Tagged Protein A to QD. To conjugate His-tagged protein to P-IM-coated QDs, the QDs (1 μM) were incubated with different ratios of His-tagged Protein A (BioVision, Inc., Milpitas, CA) or Protein A without a His-tag (Thermo Scientific, Waltham, MA) at room temperature in 10 mM phosphate buffer (pH 7.4) for 2 h. Conjugation was assessed by gel electrophoresis in a hybrid polyacrylamide-agarose gel (2% polyacrylamide and 0.5% agarose) at 4 °C.

Conjugation of Nanobody to QD. To conjugate His-tag nanobody to P-IM-coated QDs, the QDs in borate buffer were transferred to PBS and incubated with different ratios of His-tag nanobody at 4 °C for 4 h. Conjugation was measured using electrophoresis in hybrid polyacrylamide-agarose gels (2% polyacrylamide and 0.5% agarose).

Labeling of Kinesin and Single-Molecule Imaging of Labeled Kinesin. Truncated Kinesin-1 with a green fluorescent protein at the C terminus (K560-GFP) was incubated with QD−nanobodies or unconjugated QDs at a 3-fold molar excess of QDs for 20 min on ice. An imaging chamber was assembled by creating microchannels roughly 2 mm in width using double-sided tape on cleaned microscope slides. A coverslip coated with 5% PEG-Biotin/

DOI: 10.1021/jacs.5b12378
J. Am. Chem. Soc. 2016, 138, 3382−3394

95% PEG was firmly mounted to the other side of the double-sided tape. A 10 μL amount of 0.5 mg/mL Streptavidin was added to the microchannels and incubated for 5 min. Excess streptavidin was rinsed out of the microchannel. A 10 μL amount of biotinylated Hilyte488-labeled microtubule consisting of roughly 25 nM tubulins in a solution of BRB80-BSA (80 mM 1,4-piperazinediethanesulfonic acid (PIPES), 1 mM ethylene glycol tetraacetic acid (EGTA), 1 mM $MgCl_2$, and 8 mg/mL BSA, pH 6.8) containing 20 μM paclitaxel was added to the flow channel and allowed to bind for 5 min. Excess microtubules were rinsed out with BRB80-BSA containing 20 μM paclitaxel. Kinesin−QD mixture was diluted to nanomolar concentration, added to Imaging Buffer (BRB80-BSA, 1 mM tris(3-hydroxypropyl)phosphine (THP), 20 μM paclitaxel, 1 U/mL creatine kinase, 2 mM creatine phosphate, 50 nM protocatechuate-3,4-dioxygenas, 1 mg/mL protocatechuic acid), subsequently flowed into the microchannels containing microtubules, and allowed to incubate without any adenosine triphosphate (ATP) for 5 min to allow labeled kinesin to bind to the microtubules. Then 800 nM ATP in Imaging Buffer was added to the chamber to wash out the unbound kinesin and unlabeled QDs. For experiments involving measurement of step sizes, 300 nM ATP was used instead. The sample was imaged using a custom-built objective-type total internal reflection fluorescence (TIRF) microscope. QDs were excited using a 532 nm laser. For experiments that involved measuring step sizes, a 605/15 nm emission filter was added to the setup. For motility experiments, movies were collected using an Andor iXon EM-CCD camera with 150 ms exposure time and EM gain of 200 for 300 frames. To discern individual step sizes, laser power was increased 4-fold, exposure time was decreased to 100 ms, and EM gain was between 50 and 10.

Data Analysis of Motile Kinesin and Step Size Determination. The number of processive moving bright spots in each movie obtained at 800 nM ATP was counted and averaged to yield the number of motile kinesin per movie. For step size determination, motile spots in movies recorded at 300 nM ATP were cropped and single-molecule fluorescence images of QDs in each frame of the movie were fit to a 2D Gaussian function to determine its center. Since kinesin travels on a single protofilament in one direction, the set of x−y coordinate obtained from Gaussian fitting was linearized to reduce its dimensionality. The tracked position as a function of time was then fit using the SICstepfinder algorithm[36] to determine the step size from the recorded traces. The step sizes were collected from all traces, and Gaussian functions were used to fit the distribution of the step sizes.

■ ASSOCIATED CONTENT

Supporting Information

The Supporting Information is available free of charge on the ACS Publications website at DOI: 10.1021/jacs.5b12378.

Additional details on materials, instrumentation, synthesis, and characterization of ligands and quantum dots, coating methods, and single-particle tracking (PDF)

■ AUTHOR INFORMATION

Corresponding Author

*smi@illinois.edu

Author Contributions

§L.M. and C.T. contributed equally to this work.

Notes

The authors declare no competing financial interest.

■ ACKNOWLEDGMENTS

This work was supported by grants from the National Institutes of Health (R00CA153914 and R21NS087413), funds from the Mayo-Illinois Alliance, and funds from the University of Illinois at Urbana−Champaign. L.M. was supported by the National Institute of Environmental Health Sciences (NIEHS) training grant T32 ES007326. P.L. was funded from National Science Foundation (NSF) Grant 0965918 IGERT: Training the Next Generation of Researchers in Cellular and Molecular Mechanics and BioNanotechnology.

■ REFERENCES

(1) (a) Alivisatos, A. P. *J. Phys. Chem.* **1996**, *100*, 13226−13239. (b) Murray, C. B.; Kagan, C. R.; Bawendi, M. G. *Annu. Rev. Mater. Sci.* **2000**, *30*, 545−610. (c) Burda, C.; Chen, X. B.; Narayanan, R.; El-Sayed, M. A. *Chem. Rev.* **2005**, *105*, 1025−1102. (d) Smith, A. M.; Nie, S. M. *Acc. Chem. Res.* **2010**, *43*, 190−200.

(2) (a) Lee, Y. L.; Lo, Y. S. *Adv. Funct. Mater.* **2009**, *19*, 604−609. (b) Nozik, A. J.; Beard, M. C.; Luther, J. M.; Law, M.; Ellingson, R. J.; Johnson, J. C. *Chem. Rev.* **2010**, *110*, 6873−6890.

(3) (a) Anikeeva, P. O.; Halpert, J. E.; Bawendi, M. G.; Bulovic, V. *Nano Lett.* **2009**, *9*, 2532−2536. (b) Salter, C. L.; Stevenson, R. M.; Farrer, I.; Nicoll, C. A.; Ritchie, D. A.; Shields, A. J. *Nature* **2010**, *465*, 594−597. (c) Talapin, D. V.; Lee, J. S.; Kovalenko, M. V.; Shevchenko, E. V. *Chem. Rev.* **2010**, *110*, 389−458.

(4) Kairdolf, B. A.; Smith, A. M.; Stokes, T. H.; Wang, M. D.; Young, A. N.; Nie, S. *Annu. Rev. Anal. Chem.* **2013**, *6*, 143−162.

(5) (a) Ekimov, A. I.; Onushchenko, A. A. *Sov. Phys. Semicond.* **1982**, *16*, 775−778. (b) Rossetti, R.; Nakahara, S.; Brus, L. E. *J. Chem. Phys.* **1983**, *79*, 1086−1088.

(6) Yu, W. W.; Peng, X. *Angew. Chem., Int. Ed.* **2002**, *41*, 2368−2371.

(7) (a) Murray, C. B.; Norris, D. J.; Bawendi, M. G. *J. Am. Chem. Soc.* **1993**, *115*, 8706−8715. (b) Lim, S. J.; Zahid, M. U.; Le, P.; Ma, L.; Entenberg, D.; Harney, A. S.; Condeelis, J.; Smith, A. M. *Nat. Commun.* **2015**, *6*, 8210.

(8) (a) Murray, C. B.; Sun, S. H.; Gaschler, W.; Doyle, H.; Betley, T. A.; Kagan, C. R. *IBM J. Res. Dev.* **2001**, *45*, 47−56. (b) Xie, R. G.; Peng, X. G. *Angew. Chem., Int. Ed.* **2008**, *47*, 7677−7680. (c) Smith, A. M.; Nie, S. *J. Am. Chem. Soc.* **2011**, *133*, 24−26.

(9) Keuleyan, S.; Lhuillier, E.; Guyot-Sionnest, P. *J. Am. Chem. Soc.* **2011**, *133*, 16422−16424.

(10) McBride, J.; Treadway, J.; Feldman, L. C.; Pennycook, S. J.; Rosenthal, S. J. *Nano Lett.* **2006**, *6*, 1496−1501.

(11) (a) Bruchez, M.; Moronne, M.; Gin, P.; Weiss, S.; Alivisatos, A. P. *Science* **1998**, *281*, 2013−2016. (b) Chan, W. C.; Nie, S. *Science* **1998**, *281*, 2016−2018.

(12) (a) Wu, X.; Liu, H.; Liu, J.; Haley, K. N.; Treadway, J. A.; Larson, J. P.; Ge, N.; Peale, F.; Bruchez, M. P. *Nat. Biotechnol.* **2002**, *21*, 41−46. (b) Arnspang, E. C.; Brewer, J. R.; Lagerholm, B. C. *PLoS One* **2012**, *7*, e48521. (c) Zrazhevskiy, P.; Gao, X. *Nat. Commun.* **2013**, *4*, 1619. (d) Saurabh, S.; Beck, L. E.; Maji, S.; Baty, C. J.; Wang, Y.; Yan, Q.; Watkins, S. C.; Bruchez, M. P. *ACS Nano* **2014**, *8*, 11138−11146.

(13) (a) Pinaud, F.; Clarke, S.; Sittner, A.; Dahan, M. *Nat. Methods* **2010**, *7*, 275−285. (b) Liu, D. S.; Phipps, W. S.; Loh, K. H.; Howarth, M.; Ting, A. Y. *ACS Nano* **2012**, *6*, 11080−11087. (c) Zahid, M. U.; Smith, A. M. Single-Molecule Imaging with Quantum Dots. In *Optical Nanoscopy and Novel Microscopy Techniques*; Xi, P., Ed.; CRC Press: Boca Raton, FL, 2014; pp 135−160. (d) Vu, T. Q.; Lam, W. Y.; Hatch, E. W.; Lidke, D. S. *Cell Tissue Res.* **2015**, *360*, 71−86.

(14) Smith, A. M.; Nie, S. *Nat. Biotechnol.* **2009**, *27*, 732−733.

(15) Cai, E.; Ge, P.; Lee, S. H.; Jeyifous, O.; Wang, Y.; Liu, Y.; Wilson, K. M.; Lim, S. J.; Baird, M. A.; Stone, J. E.; Lee, K. Y.; Davidson, M. W.; Chung, H. J.; Schulten, K.; Smith, A. M.; Green, W. N.; Selvin, P. R. *Angew. Chem., Int. Ed.* **2014**, *53*, 12484−12488.

(16) (a) Courty, S.; Luccardini, C.; Bellaiche, Y.; Cappello, G.; Dahan, M. *Nano Lett.* **2006**, *6*, 1491−1495. (b) Smith, A. M.; Wen, M. M.; Nie, S. *Biochemist* **2010**, *32*, 12−17.

(17) (a) Swift, J. L.; Heuff, R.; Cramb, D. T. *Biophys. J.* **2006**, *90*, 1396−1410. (b) Wang, H.; Tessmer, I.; Croteau, D. L.; Erie, D. A.; Van Houten, B. *Nano Lett.* **2008**, *8*, 1631−1637. (c) Swift, J. L.; Cramb, D. T. *Biophys. J.* **2008**, *95*, 865−876. (d) Ko, S. H.; Gallatin, G. M.; Liddle, J. A. *Adv. Funct. Mater.* **2012**, *22*, 1015−1023.

(18) (a) Lidke, D. S.; Nagy, P.; Heintzmann, R.; Arndt-Jovin, D. J.; Post, J. N.; Grecco, H. E.; Jares-Erijman, E. A.; Jovin, T. M. *Nat.*

DOI: 10.1021/jacs.5b12378
J. Am. Chem. Soc. 2016, 138, 3382−3394

Biotechnol. **2004**, *22*, 198−203. (b) You, C. J.; Wilmes, S.; Beutel, O.; Lochte, S.; Podoplelowa, Y.; Roder, F.; Richter, C.; Seine, T.; Schaible, D.; Uze, G.; Clarke, S.; Pinaud, F.; Dahan, M.; Piehler, J. *Angew. Chem., Int. Ed.* **2010**, *49*, 4108−4112.
(19) (a) Susumu, K.; Uyeda, H. T.; Medintz, I. L.; Pons, T.; Delehanty, J. B.; Mattoussi, H. *J. Am. Chem. Soc.* **2007**, *129*, 13987−13996. (b) Liu, W.; Howarth, M.; Greytak, A. B.; Zheng, Y.; Nocera, D. G.; Ting, A. Y.; Bawendi, M. G. *J. Am. Chem. Soc.* **2008**, *130*, 1274−1284.
(20) Dubertret, B.; Skourides, P.; Norris, D. J.; Noireaux, V.; Brivanlou, A. H.; Libchaber, A. *Science* **2002**, *298*, 1759−1762.
(21) Aldana, J.; Wang, Y. A.; Peng, X. G. *J. Am. Chem. Soc.* **2001**, *123*, 8844−8850.
(22) Zhang, F.; Lees, E.; Amin, F.; Rivera Gil, P.; Yang, F.; Mulvaney, P.; Parak, W. J. *Small* **2011**, *7*, 3113−3127.
(23) Smith, A. M.; Nie, S. *J. Am. Chem. Soc.* **2008**, *130*, 11278−11279.
(24) (a) Palui, G.; Na, H. B.; Mattoussi, H. *Langmuir* **2012**, *28*, 2761−2772. (b) Giovanelli, E.; Muro, E.; Sitbon, G.; Hanafi, M.; Pons, T.; Dubertret, B.; Lequeux, N. *Langmuir* **2012**, *28*, 15177−15184. (c) Xu, J. M.; Ruchala, P.; Ebenstain, Y.; Li, J. J.; Weiss, S. *J. Phys. Chem. B* **2012**, *116*, 11370−11378. (d) Liu, W. H.; Greytak, A. B.; Lee, J.; Wong, C. R.; Park, J.; Marshall, L. F.; Jiang, W.; Curtin, P. N.; Ting, A. Y.; Nocera, D. G.; Fukumura, D.; Jain, R. K.; Bawendi, M. G. *J. Am. Chem. Soc.* **2010**, *132*, 472−483. (e) Zhang, P.; Liu, S.; Gao, D.; Hu, D.; Gong, P.; Sheng, Z.; Deng, J.; Ma, Y.; Cai, L. *J. Am. Chem. Soc.* **2012**, *134*, 8388−8391. (f) Han, H. S.; Martin, J. D.; Lee, J.; Harris, D. K.; Fukumura, D.; Jain, R. K.; Bawendi, M. *Angew. Chem., Int. Ed.* **2013**, *52*, 1414−1419. (g) Susumu, K.; Oh, E.; Delehanty, J. B.; Pinaud, F.; Gemmill, K. B.; Walper, S.; Breger, J.; Schroeder, M. J.; Stewart, M. H.; Jain, V.; Whitaker, C. M.; Huston, A. L.; Medintz, I. L. *Chem. Mater.* **2014**, *26*, 5327−5344.
(25) Chakraborty, A. K.; Golumbfskie, A. J. *Annu. Rev. Phys. Chem.* **2001**, *52*, 537−573.
(26) (a) Pelaz, B.; Jaber, S.; de Aberasturi, D. J.; Wulf, V.; Aida, T.; de la Fuente, J. M.; Feldmann, J.; Gaub, H. E.; Josephson, L.; Kagan, C. R.; Kotov, N. A.; Liz-Marzán, L. M.; Mattoussi, H.; Mulvaney, P.; Murray, C. B.; Rogach, A. L.; Weiss, P. S.; Willner, I.; Parak, W. J. *ACS Nano* **2012**, *6*, 8468−8483. (b) Kim, C.; Galloway, J. F.; Lee, K. H.; Searson, P. C. *Bioconjugate Chem.* **2014**, *25*, 1893−1901. (c) Han, H.-S.; Niemeyer, E.; Huang, Y.; Kamoun, W. S.; Martin, J. D.; Bhaumik, J.; Chen, Y.; Roberge, S.; Cui, J.; Martin, M. R.; Fukumura, D.; Jain, R. K.; Bawendi, M. G.; Duda, D. G. *Proc. Natl. Acad. Sci. U. S. A.* **2015**, *112*, 1350−1355.
(27) (a) Goldman, E. R.; Medintz, I. L.; Hayhurst, A.; Anderson, G. P.; Mauro, J. M.; Iverson, B. L.; Georgiou, G.; Mattoussi, H. *Anal. Chim. Acta* **2005**, *534*, 63−67. (b) Lao, U. L.; Mulchandani, A.; Chen, W. *J. Am. Chem. Soc.* **2006**, *128*, 14756−14757. (c) Dennis, A. M.; Sotto, D. C.; Mei, B. C.; Medintz, I. L.; Mattoussi, H.; Bao, G. *Bioconjugate Chem.* **2010**, *21*, 1160−1170. (d) Kotagiri, N.; Li, Z.; Xu, X.; Mondal, S.; Nehorai, A.; Achilefu, S. *Bioconjugate Chem.* **2014**, *25*, 1272−1281. (e) Bilan, R.; Fleury, F.; Nabiev, I.; Sukhanova, A. *Bioconjugate Chem.* **2015**, *26*, 609−624.
(28) Gujraty, K. V.; Yanjarappa, M. J.; Saraph, A.; Joshi, A.; Mogridge, J.; Kane, R. S. *J. Polym. Sci., Part A: Polym. Chem.* **2008**, *46*, 7249−7257.
(29) Nag, A.; Kovalenko, M. V.; Lee, J.-S.; Liu, W.; Spokoyny, B.; Talapin, D. V. *J. Am. Chem. Soc.* **2011**, *133*, 10612−10620.
(30) Schollbach, M.; Zhang, F.; Roosen-Runge, F.; Skoda, M. W. A.; Jacobs, R. M. J.; Schreiber, F. *J. Colloid Interface Sci.* **2014**, *426*, 31−38.
(31) (a) Baskin, J. M.; Prescher, J. A.; Laughlin, S. T.; Agard, N. J.; Chang, P. V.; Miller, I. A.; Lo, A.; Codelli, J. A.; Bertozzi, C. R. *Proc. Natl. Acad. Sci. U. S. A.* **2007**, *104*, 16793−16797. (b) Laughlin, S. T.; Baskin, J. M.; Amacher, S. L.; Bertozzi, C. R. *Science* **2008**, *320*, 664−667.
(32) Boeneman, K.; Deschamps, J. R.; Buckhout-White, S.; Prasuhn, D. E.; Blanco-Canosa, J. B.; Dawson, P. E.; Stewart, M. H.; Susumu, K.; Goldman, E. R.; Ancona, M.; Medintz, I. L. *ACS Nano* **2010**, *4*, 7253−7266.
(33) Dennis, A. M.; Bao, G. *Nano Lett.* **2008**, *8*, 1439−1445.
(34) Wang, Y.; Cai, E.; Rosenkranz, T.; Ge, P.; Teng, K. W.; Lim, S. J.; Smith, A. M.; Chung, H. J.; Sachs, F.; Green, W. N.; Gottlieb, P.; Selvin, P. R. *Bioconjugate Chem.* **2014**, *25*, 2205−2211.
(35) Svoboda, K.; Schmidt, C. F.; Schnapp, B. J.; Block, S. M. *Nature* **1993**, *365*, 721−727.
(36) Kalafut, B.; Visscher, K. *Comput. Phys. Commun.* **2008**, *179*, 716−723.

DOI: 10.1021/jacs.5b12378
J. Am. Chem. Soc. 2016, 138, 3382−3394